Development of MIL-101(Cr)/GrO composites for adsorption heat pump applications

Elsayed, Eman; Wang, Haiyan; Anderson, Paul A.; Al-dadah, Raya; Mahmoud, Saad; Navarro, Helena; Ding, Yulong; Bowen, James

DOI:
10.1016/j.micromeso.2017.02.020

Document Version
Peer reviewed version

Citation for published version (Harvard):
Elsayed, E, Wang, H, Anderson, PA, Al-dadah, R, Mahmoud, S, Navarro, H, Ding, Y & Bowen, J 2017, 'Development of MIL-101(Cr)/GrO composites for adsorption heat pump applications', *Microporous and Mesoporous Materials*, vol. 244, pp. 180-191. https://doi.org/10.1016/j.micromeso.2017.02.020

Accepted Manuscript

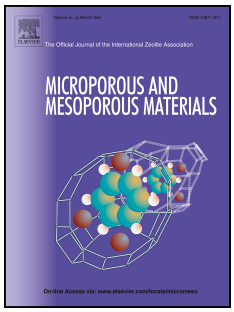

Development of MIL-101(Cr)/GrO composites for adsorption heat pump applications

Eman Elsayed, Haiyan Wang, Paul A. Anderson, Raya Al-Dadah, Saad Mahmoud, Helena Navarro, Yulong Ding

PII: S1387-1811(17)30061-6

DOI: 10.1016/j.micromeso.2017.02.020

Reference: MICMAT 8130

To appear in: *Microporous and Mesoporous Materials*

Received Date: 31 October 2016

Revised Date: 7 January 2017

Accepted Date: 6 February 2017

Please cite this article as: E. Elsayed, H. Wang, P.A. Anderson, R. Al-Dadah, S. Mahmoud, H. Navarro, Y. Ding, Development of MIL-101(Cr)/GrO composites for adsorption heat pump applications, *Microporous and Mesoporous Materials* (2017), doi: 10.1016/j.micromeso.2017.02.020.

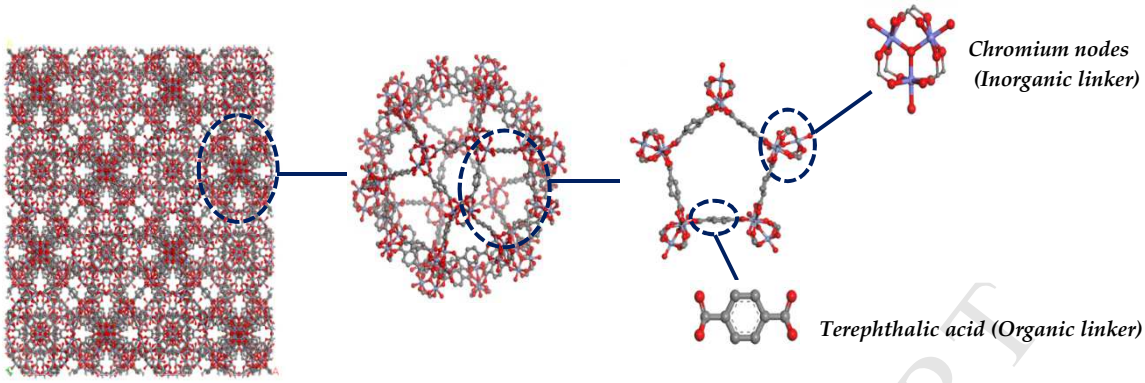

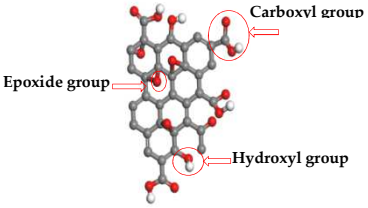

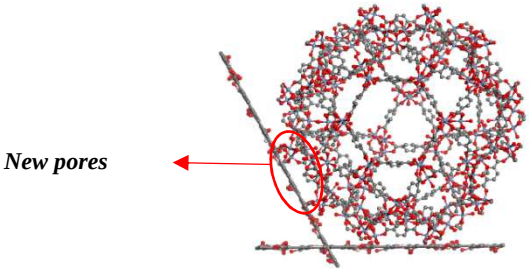

Development of MIL-101(Cr) / GrO Composites for adsorption heat pump applications

Eman Elsayed[a,b,*], Haiyan Wang[a,c], Paul A. Anderson[b], Raya AL-Dadah[a], Saad Mahmoud[a] , Helena Navarro[d], Yulong Ding[d]

[a] School of Mechanical Engineering, University of Birmingham, Birmingham, B15 2TT, UK.
[b] School of Chemistry, University of Birmingham, Birmingham, B15 2TT, UK.
[C] College of Chemical Engineering, Nanjing Tech University, Nanjing, 210009, China.
[d]Birmingham Centre for Energy Storage, School of Chemical Engineering, University of Birmingham, UK.
* Corresponding author. E-mail: EXH496@student.bham.ac.uk ; Tel.: 07477373797.

Abstract

Adsorption heat pumps can be used for generating heating, cooling, seasonal energy storage and water desalination applications. Metal-organic frameworks (MOFs) are hybrid porous materials with high surface area and superior adsorption characteristics compared to conventional adsorbents. MIL-101(Cr) has a large pore size with water vapour adsorption capacity up to 1.5 g_{H2O} g_{ads}^{-1} and high cyclic stability thus has the potential to be used in adsorption heat pumps. This work investigates the enhancement of the thermal conductivity and water adsorption characteristics of MIL-101(Cr) using hydrophilic graphene oxide. Two methods have been used to develop MIL-101(Cr)/GrO composites. The first method was through incorporating the GrO during the synthesis process of MIL-101(Cr) while the other was through the physical mixing. The composites and MIL-101(Cr) were characterized in terms of their structure, water adsorption uptake, BET surface area, particle size, thermal gravimetric analysis, SEM images and thermal conductivity measurements. Results showed that introducing low amounts of GrO (<2%) to the neat MIL-101(Cr) enhanced the water adsorption characteristics at high relative pressure but enhanced the heat transfer properties by 20-30% while using more than 2% of GrO reduced the adsorption water uptake but significantly enhanced the thermal conductivity by more than 2.5 folds.

Keywords: Metal–organic framework**,** characterization, adsorption, heat pump, thermal conductivity.

1. Introduction

The concept of adsorption heat pump cycle is based on the phenomenon that when the working fluid is evaporated; taking evaporation heat Q_{evap} from the surroundings, a useful cold effect is produced when the cycle is used as a chiller. When vapour of the working fluid is adsorbed into a porous material, generating adsorption heat Q_{ads} this can be released to the environment when the system is used in a heat pump application. The main advantages of adsorption systems are that they can be driven by low temperature heat sources such as solar energy or waste heat, they are environmentally friendly as there is almost no CO_2 emissions, the simplicity of the system and also the long operating life.

Metal–organic frameworks (MOFs) have attracted extensive attention due to their ultrahigh surface area, tunable pore structures and surface functionality where functional groups such as -OH and -NH_2 can be incorporated in the structure to improve the performance. These exceptional properties, endow MOFs with great potential in a number of applications such as catalysis [1], gas separation and storage [2] and

sensors [3]. MOFs have been investigated in adsorption heat pump applications where they showed good performance. *Jeremias et al* [4] synthesized a coating of microporous aluminium fumarate on a metal substrate *via* the thermal gradient approach, which was stable for over 4500 water vapour adsorption/desorption cycles showing its potential to be used in heat transformation applications. *Rezk et al* [5, 6] compared the performance of HKUST-1 and MIL-100(Fe) to silica gel showing that HKUST-1 outperformed silica gel RD-2060 with 93.2% higher water uptake, while MIL-100(Fe) showed an increase of 26.8%. The authors suggested that using these two MOFs can lead to a considerable increase in the refrigerant flow rate, the cooling capacity and eventually reduction in the size of the adsorption system. The MIL-100 family showed adsorption capabilities of 0.75 $g_{H2O}\ g_{ads}^{-1}$ for MIL-100(Fe) and 0.5 $g_{H2O}\ g_{ads}^{-1}$ for MIL-100(Al), in addition to the small hysteresis and the very good cycle stability, make both MIL-100(Al and Fe) very suitable candidates for thermally driven heat pumps and adsorption chillers [7]. *Henninger et al* [8] compared another MOF material, ISE-1, to silica gel and 5 types of zeolites. ISE-1 outperformed all the other 6 materials at low desorption temperatures and showed a stable performance over 10 successive adsorption/ desorption cycles, making it a promising candidate for heat transformation applications. A later study by *Henninger et al* [9] investigated the potential of MIL-100(Fe), MIL-100(Cr), HKUST-1, ISE-1, Basolite C300, Basolite A100 and Basolite F300. It was concluded that the high hydrothermal stability of these materials (except for HKUST-1), and the ability to change their water vapour capacity, by varying the organic linker and the metal cluster resulting in tunable properties, make them a promising class of materials to be used in adsorption heat transformation processes.

MIL-101(Cr), is a mesoporous material with two types of cages of 29 and 34 Å diameter and is considered to be one of the most investigated MOFs due to its high pore volume of $2cm^3g^{-1}$, the exceptionally high surface area of 4500 m^2g^{-1}, high water uptake of 1−1.43 $g_{H2O}.g_{ads}^{-1}$ (at high relative pressure > 0.35) and high cyclic stability [9-13]. The adsorption performance of MIL-101(Cr) and other MOF materials was further improved by means of recombination with expanded natural graphite (ENG), multi-walled carbon nanotubes (MWCNT), graphite oxide (GO) and graphene oxide (GrO). The addition of expanded natural graphite (ENG) to MOF-5 [14] lowered the hydrogen storage capacity, while the addition of zeolite-templated carbon to MIL-101(Cr) showed H_2 uptake enhancement of 43% [15]. *Kumar et al* [14] synthesized a composite of a ZIF-8 MOF and graphene oxide where the BET surface area of the composites decreased with increasing GO content. The CO_2 adsorption performances of the synthesized composites showed an enhanced behaviour up to 72wt% in the composite with 20wt%GO (ZG-20). The incorporation of graphite oxide into several MOFs [MOF-5, HKUST-1 and MIL-100(Fe)] also produced an enhanced performance for the adsorption of NH_3, H_2S and NO_2 [17-21]. The CO_2 and CH_4 adsorption performance of HKUST-1 [22] and MIL-53(Cr) [23] were enhanced through using MWCNT. Similarly, graphene oxide (GrO) has been incorporated into MIL-101(Cr), showing an increase of 44.4% for the adsorption of acetone compared to the neat material [24]. Another composite of MIL-101(Cr) but with GO showed an increase of 25–29% in the n-alkanes adsorption capacity compared to the neat material [25]. A comparison between the water adsorption capacity of MIL-101(Cr) and a composite

MIL-101(Cr) and graphite oxide showed that the exceptional water uptake of 1.22 g_{H2O} g_{ads}^{-1} was even increased to reach 1.58 g_{H2O} g_{ads}^{-1} for the 6% GO composite [26]. However, these exceptional properties of MOFs come with the price of extremely low thermal conductivity due to their large pore sizes and high free volumes. The low thermal conductivity limits the ability of the heat transfer processes to reach the desired operating temperatures quickly during both the adsorption and desorption phases. A molecular simulation study was conducted by *Zhang et al* [27] to calculate the thermal conductivity of zeolitic imidazolate framework (ZIF-8). It was reported that the thermal conductivity varies from 0.165 to 0.190 W (m K) $^{-1}$ in the temperature range of 300 to 1000 K. The thermal conductivity has been experimentally measured for MOF-5 [28] and found to be only 0.1 W (m K)$^{-1}$ at room temperature. The low thermal conductivity was enhanced through the use of the thermally conductive Expanded Natural Graphite (ENG); the additions of 10 wt % ENG resulted in a five folds enhancement in the thermal conductivity relative to neat MOF-5, increasing it from 0.10 to 0.56 W (m K) $^{-1}$.

Graphene oxide is a derivative of the highly thermally conductive graphene which is one-atom-thick planar sheets of bonded carbon atoms that are densely packed in a hexagonal crystal lattice. The oxidation of the graphene gives a graphene layer with functional groups such as epoxide (-O-), hydroxyl (-OH), and carboxyl (-COOH). The thermal properties of graphene oxide and its reduced form have been used in multi-wall carbon nanotube (MWCNT)/epoxy composites [29], organic phase change materials (n-eicosane) in silica microcapsules [*30*], producing nanofluids with ethylene glycol [31], polymer (epoxy) for printed electronics [32] and epoxy resin (brand Epon862) [*36*].

The thermal properties in addition to the hydrophilicity (as the oxygen in the epoxide group strongly binds to water molecules through hydrogen bonding interactions) of the graphene oxide have motivated the authors to assess the effect of GrO on the water adsorption characteristics and the thermal conductivity of a series of MIL-101(Cr)/GrO composites.

2. Experimental work

All chemicals were of reagent-grade quality obtained from commercial sources. Chromium nitrate ($Cr(NO_3)_3.9H_2O$, Acros organics, 99%), terephthalic acid H_2BDC ($C_6H_4(CO_2H)_2$, Sigma-Aldrich, 98%), tetramethyl ammonium hydroxide (TMAOH, $(CH_3)_4NOH$, Sigma-Aldrich, 25%), graphene oxide (Sigma-Aldrich) and absolute ethanol (Fisher Scientific) were used without further purification.

i. Synthesis of MIL-101(Cr)

MIL-101(Cr) was synthesized *via* a hydrothermal method reported by [*34*] where terephthalic acid (H_2BDC, 4 mmol) was added to an alkali solution of tetramethyl ammonium hydroxide (TMAOH, 16 ml) and stirred at room temperature for 10 minutes, then $Cr(NO_3)_3.9H_2O$ (4 mmol) was added to the mixture and stirred for another 20 minutes. The resulting mixture was transferred into a 45 ml Teflon-lined autoclave and heated at 453 K for 24 h. After cooling slowly to ambient temperature, a solution of fine green powder as the major product was obtained with a significant amount of recrystallized H_2BDC. To eliminate the traces of carboxylic acid, the mixture was first filtered using a large pore glass filter. The water and the fine powder of MIL-101(Cr) passed through the filter while the free acid stayed on the glass

filter. After that, the solution was centrifuged to separate the MIL-101(Cr) particles; the collected solids were then suspended in absolute ethanol, stirred at 333 K for 1hr and centrifuged again. This process was repeated at least 2 times. The collected solids were once again suspended in water, stirred at 333 K for 1hr and finally the green powder was separated from the solution using a small pore filter paper. The product was dried in air at room temperature.

ii. Synthesis of MIL-101(Cr)/GrO composites

Composites were synthesized through two different routes: the first route was through the mixing of MIL-101(Cr) and graphene oxide to obtain GrO_physical composites. To ensure the complete homogeneity between MIL-101(Cr) and GrO particles, the GrO was added in different ratios to the pre-synthesized MIL-101(Cr) with few drops of water. The mixture was briefly sonicated, filtered and left to dry in air. The other route was through incorporation of graphene oxide into MIL-101(Cr) during synthesis process. Typically, the composites were prepared by using the same method employed in the synthesis of MIL-101(Cr). After thorough mixing of the reactants (chromium nitrate, tetramethyl ammonium hydroxide and terephthalic acid), the GrO was added in different ratios based on the expected mass of the product. The suspension was sonicated for 30 minutes and then stirred at 313 K for 15 minutes. Finally, it was transferred into a 45 ml Teflon-lined autoclave and heated at 453 K for 24 h. After cooling slowly to the ambient temperature, the product was purified in the same manner as the neat MIL-101(Cr) obtaining the GrO_synthesis composites.

iii. Material characterization

The neat material MIL-101(Cr) and the composites were characterized using powder X-ray diffraction (XRD), BET surface area through nitrogen adsorption, water adsorption characteristics, particle size, thermal gravimetric analysis (TGA), Raman spectroscopy, Scanning Electron Microscopy (SEM) and thermal conductivity measurements.

The powder XRD patterns were measured using a Siemens D5005 diffractometer with Cu Kα radiation (1.5418 Å). The samples were scanned from 3 to 30° 2θ with a step size of 0.02°.

Water adsorption characteristics were measured using a dynamic vapour sorption (DVS) gravimetric analyser (Advantage DVS, Surface Measurement Systems, UK) using the methodology previously described [5].

The N_2 adsorption isotherm at 77 K was used to measure the BET surface area [35] using a Quantachrome NOVA surface area analyser. Each sample was evacuated at 393 K. The BET surface area was obtained in the relative pressure range from 0.03 to 0.3, the total pore volume was calculated at a relative pressure of 0.95, the micropore volume was calculated using t-plot method and the pore size distribution was calculated using DFT method. The mesoporous volume can be calculated as the difference between the total pore volume and the micropore volume.

The particle size was measured using a Delsa™Nano Particle Size analyser using water as the solvent.

Thermal gravimetric analysis (TGA) was used to investigate the thermal stability of the materials using a Perkin Elmers Pyris 1.

Raman spectroscopy was carried out using Renishaw in Via Raman Microscope laser (λ= 633 nm).

Scanning electron microscopy (SEM) images were taken using a CFEI Quanta 3D FEG FIB-SEM.

The thermal diffusivity was measured using a NETZSCH-LFA 427 in a temperature range of 303K to 473 K. The samples were evacuated at 453 K under vacuum for 6 hours, pressed under a pressure of 20MPa to give pellets with an average diameter of 12.9 mm and 1.6 mm average thickness. The pellets produced were coated with graphite to improve the light absorption.

The specific heat capacity was measured in the same temperature range using a METTLER TOLEDO DSC2.

3. Results and Discussion

i. Powder XRD

The powder X-ray diffraction (XRD) patterns of GrO, neat MIL-101(Cr), composites prepared through the physical mixture route and composites prepared through the incorporating route are all shown in **Fig.1**. It can be noticed that the peaks of MIL-101(Cr) were preserved as it is the major component of all the composites. This indicates that during the synthesis process of the composites, the presence of the GrO did not prevent the formation of the MIL-101 crystals even though a notable decrease in the intensity of the peaks for the composites was observed. This may be attributed to the partial distortion of the MIL-101(Cr) structure owing to presence of GrO during the crystal growth process [36]. From the figure, GrO is amorphous as there is only one visible peak at 11° which did not appear in any of the composite patterns. A similar behaviour was attributed to the low content of GrO used [20] or its high dispersion [17,18].

ii. Nitrogen adsorption isotherms and BET surface area

The N_2 adsorption isotherms at 77 K (**Fig.2**) showed that the 2%GrO_synthesis composite had the highest capacity. The measured surface areas are illustrated in **Table 1.**

The highest surface area was observed for the 2%GrO_synthesis composite which was more than 6% higher than the neat MIL-101(Cr). This supports the suggestion that the 2%GrO_synthesis composite had additional porosity as the total pore volume increased from 1.75 to 2.14 $cm^3\ g^{-1}$. The increase in the pore volume was due to the increase in the mesopores volume which increased from 1.33 to 1.69 $cm^3\ g^{-1}$ while a negligible increase was observed in case of the micropore volume.

Such increase in the surface area and the pore volume is due to the interaction between the framework and the GrO structure through the coordination between the epoxy groups of the GrO and the metal ions from the structure (**Fig.3**). Higher GrO showed a lower surface area which may be due to that in the spherical crystal shape of MIL-101(Cr), GrO sheets have more than one possible orientation to attach to the crystal. This not only restrains the attachment of further proper attachment of GrO layers but also cause the distortion of the MIL structure (**Fig. 3**). This caused the surface area to decrease from 3674 $m^2\ g^{-1}$ for the 2%GrO composite to only 2810 $m^2\ g^{-1}$ for 5%GrO.

For the physical composites, a significant reduction in the surface area and the pore volume was noticed. This supports the suggestion that the GrO may block the pores of the MIL-101(Cr) and hence the pore volume is reduced. **Fig. 4** shows the pore size distribution calculated from the DFT method. It is evident that pore size distribution curves of the physical and synthesis composites were similar to the parent material. It can be noticed that the 2%GrO_synthesis composite has a higher pore volume than the parent material while the rest of the composites are with lower pore volume. This was shown as well in the measurement of the surface area and total pore volume.

Table 1 surface area of MIL-101(Cr) and GrO composite.

Material	BET surface area (m^2g^{-1})	Total pore volume (cm^3g^{-1})	Mesopores volume (cm^3g^{-1})	Micropores volume (cm^3g^{-1})
GrO	Nil	Nil	Nil	Nil
Neat MIL-101(Cr)	3460	1.753	1.33	0.41
0.5%GrO_synthesis	3137.8	1.641	1.39	0.24
0.5%GrO_physical	2608.5	1.346	1.22	0.12
1%GrO_synthesis	3028.1	1.619	1.32	0.29
1%GrO_physical	2425.7	1.265	1.11	0.15
2%GrO_synthesis	3674	2.14	1.69	0.45
2%GrO_physical	2077	1.035	0.80	0.23
5%GrO_synthesis	2810	1.879	1.56	0.28
5%GrO_physical	2626	1.33	1.05	0.31

iii. Water adsorption characteristics

Fig.5 shows the water adsorption isotherms of the neat material and the composites which exhibited type IV isotherm. At low relative pressure (≤0.4), the water vapour adsorption is mainly due to the presence of unsaturated metal centres (UMCs). These UMCs are metal binding sites formed after the removal of axial ligands from metal atoms attracting water molecules and offering extra binding sites to the guest molecules, especially at low pressure values. Nevertheless, the limited water uptake is related to the dominant effect of the hydrophobicity of the organic linker. At higher relative pressure (0.4-0.5), a steep increase in the water uptake took place due to the capillary condensation which usually takes place in mesoporous materials. Because of this phenomenon, most adsorption isotherms of large pore materials are accompanied by a hysteresis loop between the adsorption and desorption branches [37-38]. At high relative pressure (≥0.5), the pores are almost filled exhibiting a stable uptake. Also, it can be observed, all the physical mixtures have a lower water vapour uptake than the neat material, which may be attributed to the low uptake of GrO in addition to other factors such as the lower crystallinity and the potential pores blocking by the GrO. It was observed that the two synthesized composites (2%GrO_synthesis and 5%GrO_synthesis) showed an increased uptake in the high relative pressure range, which suggests that the oxygen functionalities of GrO (hydroxyl, carboxyl, epoxy) were able to coordinate to the metallic centres of the MIL-101(Cr) structure and hence new pores were created at the interface of the structure and the graphene layers. Such conclusion was in good agreement with the increase in the mesopore volume of the two composites. The 2%GrO_synthesis composite showed a maximum water uptake of 1.56 $g_{H2O}.g_{ads}^{-1}$ while the 5%GrO_synthesis reached 1.47 $g_{H2O}\ g_{ads}^{-1}$. It can be concluded that the GrO

content of 2 wt% is considered as an optimum concentration as increasing or decreasing the GrO would adversely affect the water uptake. This may be attributed to the fact that GrO is non-porous material and may cause pore blocking, and thus it will lower the accessible surface area and pore volume of the composites if more GrO is incorporated into MIL-101(Cr). As a result, it cannot improve the water vapour capacity of a composite any further [26].

Another explanation could be adopted from a previous study done on the incorporation of GO on MIL-100(Fe) [20]. With the spherical shape of the pores of MIL-101(Cr) as shown in **Fig.3**, the graphene layers have more than two modes of coordination to the MOF units. As well as that, the presence of a high amount of GrO creates additional constraints for growth of the crystal during the synthesis process (**Fig.3**) and therefore, the graphene layers may prevent the proper building of the MIL-101(Cr) structure by blocking the assembly of several cages into a zeolite-like network. At a very low GrO content, the probability of having two or more graphene layers linked to the MIL cages is reduced but may not be sufficient to produce the coordination bonds with the MIL structure (as in 1%GrO and 0.5%GrO composites), hence the water adsorption capacity is not improved. Not only that but increasing the GrO content may cause a partial distortion of the structure which may narrow the pore size of MIL-101 (Cr) [15]. In the case of the physical composites, introducing the GrO appears to adversely affect the adsorption capacity of the MIL-101(Cr). This may be due to the GrO blocking some of the pores and hence decreasing its capacity for water vapour.

The effect of incorporating GrO on adsorption cycle performance can be better understood using a comparison between the 2%GrO_synthesis composite and the parent MIL-101(Cr). For an adsorption system working at an adsorption and a condenser temperature of 298 K, an evaporation temperature of 293 K and a desorption temperature of only 343 K which means working at a relative pressure of 0.75 in the adsorption phase and 0.1 in the desorption phase. Based on the equilibrium data, the water loading difference, which is the difference between the amount of water adsorbed in the adsorption process and the amount of water remained in the pores after the desorption process, in the case of the parent material is 1.36 $g_{H2O}.g_{ads}^{-1}$ while it is 1.33 $g_{H2O}.g_{ads}^{-1}$ in the case of the composite. Those values are much higher than that of other types of MOFs at the same operating conditions. Aluminium fumarate can have a water difference load of 0.45 $g_{H2O}\ g_{ads}^{-1}$ [4] while MIL-100(Al) has 0.4 $g_{H2O}\ g_{ads}^{-1}$ and MIL-100(Fe) has 0.65 $g_{H2O}\ g_{ads}^{-1}$ [7]. The water loading difference is a crucial parameter affecting the performance of the adsorbent in any adsorption system as increasing it will increase the efficiency of the adsorption system. This shows that introducing the GrO kept the same high water adsorption characteristics at that temperature range. At higher evaporation temperatures, which corresponds to a higher relative pressures, the 2%GrO_synthesis composite is expected to outperform the neat material. The above data show the great potential of MIL-101(Cr) and its composites in adsorption heat pump application.

iv. Particle size measurement:

The particle size of samples was measured by placing a small amount of dry samples and suspend it in water, sonicated briefly and placed for analysis. Each measurement was repeated 5 times to give the average particle size. **Table 2** shows the particle size distribution of every sample D50 (particle size reaching 50% of the cumulative volume)**.**

Regarding the particle size of the synthesis composites, it can be observed that increasing the content of GrO decreased the size of the particles produced. This supports the suggestion that the presence of GrO may create constraints on the crystal growth during the synthesis process as shown in **Fig. 3**. Nevertheless, the particle size of the 5%GrO_synthesis composite was found to have a similar size to the neat material. This may be due to the partial distortion of the MIL structure or that the formed crystals restacked into larger particles.

For the physical mixing samples, it can be noticed that all the samples have almost the same particle size with a slightly higher diameter than the neat MIL-101(Cr) particles. This may be attributed to that the presence GO caused the coating of MIL crystals and the agglomeration to form larger particles.

Table 2 Particle size of MIL-101(Cr) and GrO composites.

Material	D50 (μm)
Neat MIL-101(Cr)	0.92
GrO	1.48
0.5%GrO_synthesis	0.70
0.5%GrO_physical	1.11
1%GrO_synthesis	0.58
1%GrO_physical	0.98
2%GrO_synthesis	0.68
2%GrO_physical	1.00
5%GrO_synthesis	0.94
5%GrO_physical	1.10

v. Thermal gravimetric analysis (TGA):

The analysis was carried out in the temperature range from 298 K to 873 K, using a heating rate of 10 $K.min^{-1}$ under a nitrogen flow (60 $mL.min^{-1}$).

Fig.6 shows the TGA patterns of the neat MIL-101(Cr), GrO and the different composites showing there are three stages of weight loss. The first stage where the material loses its guest or free water trapped in the pores. The parent MIL-101(Cr) shows that it loses more than 50% of its weight at 410 K while the synthesis_composites show less adsorbed water that can be lost at lower temperatures. The physical_composites showed a much lower weight loss than the neat material and the other composites. The second stage is due to the departure of the coordinated water molecules where a relatively low weight loss takes place. This stage took place in the temperature range of 410 K to 610 K for the neat material and was shifted to higher temperatures in case of composites. This indicates that the composites show improved thermal stability over the neat material. The final stage is where the weight loss is due to the combustion of the terephthalic acid and the decomposition of the structure.

vi. Raman spectroscopy:

Fig.7 shows the Raman spectra of MIL-101(Cr), GrO, synthesis composites and physical composites. The GrO exhibited two characteristic bands at 1337 cm^{-1} and 1587 cm^{-1} while MIL-101(GrO) had five characteristic bands at 1611, 1454, 1142, 864 and 632 cm^{-1}. In the synthesis composites, it is evident that the synthesis composites preserved the main bands of the MIL-101(Cr) with the presence of a small shoulder before the 1454 cm^{-1} band as the GrO increased. This proves the successful incorporation of GrO into the MIL structure without preventing the MIL crystal formation.

In case of the physical composites, the main bands of MIL-101(Cr) were found to be very weak with the two characteristic bands of the GrO at 1337 cm^{-1} and 1587 cm^{-1} overlapping the MIL bands at 1611, 1454 cm^{-1}. This may be attributed to that the grains of MIL-101(Cr) are being sheltered by the GrO layers. A similar behaviour was observed by *Zhou et al.* [24].

vii. Scanning electron microscopy (SEM):

Fig. 8 shows SEM images of MIL-101(Cr), GrO and the composites. The neat material had a well-defined octahedral crystals **(a)** while the evident wrinkles on the GrO sheet **(b)** have been ascribed to the presence of the carboxylate, epoxide and hydroxyl functional groups [29]. Regarding the synthesis composites, it can be observed that as the GrO content increased to reach 0.5, 1 and 2%, the size of the crystals started to decrease which was observed from the particle size measurement. Also, as the GrO content increased, the crystals slowly started to lose their octahedral shape. This may be attributed to the additional constraints on the crystal growth of the MIL-101 crystals during the synthesis of the composites caused by the presence of the GrO leading to a partial distortion in the crystal morphology. As the concentration increased to 5%, the crystals became irregular as the crystals restacked into larger particles.

The physical composites showed a less smooth surface than that of the parent MIL-101(Cr). This may be due the presence of graphene layers covering the MIL particles.

viii. Thermal conductivity

One of the main drawbacks of MOFs in general and MIL-101(Cr) in particular is the poor thermal conductivity due to the large pore size and high free volumes. Such property is crucial in adsorption and desorption processes. **Fig.9** shows the thermal conductivity of the material as a function of temperature. It can be seen that the thermal conductivity of neat MIL-101(Cr) is 0.05 W (m K) $^{-1}$ at 303 K and it increased linearly to reach 0.103 W (m K) $^{-1}$ at 473 K. The effect of the presence of graphene oxide at different ratios was also investigated. Despite the presence of the oxygen atoms, which typically enhances phonon scattering, the enhancement of the thermal conductivity observed can be attributed to the increase in the interlayer coupling due to covalent interactions between the oxygen atom of the GrO and the MIL-101(Cr) framework [39].

In the case of the 0.5%GrO and 1%GrO composites, the thermal conductivity was almost the same as the neat material. Increasing the GrO content to 2wt%, increased the thermal conductivity by 20−30%. As the GrO increased to 5% in the physical composite, the thermal conductivity was enhanced by a factor of 2.5

to reach 0.126 W (m K) $^{-1}$ at 303 K and 0.243 W (m K) $^{-1}$ at 473 K. On the other hand, increasing the GrO content to 5% in the synthesis composites adversely affected the thermal conductivity, a similar behaviour was observed by *Im et al* [29]. It was attributed to the insufficient interface between the GrO and the parent material which increased the interfacial resistance. Another reason is the crystal defects caused by the presence of the GrO that may affected the physical properties of the material.

Conclusions

MIL-101(Cr) has exceptional high water adsorption uptake of around 1.47 g_{H2O} g_{ads}^{-1} due to its high surface area and pore volume. Nevertheless, like most porous materials, it suffers from poor thermal conductivity due to the large pore volume. Therefore, this work investigated the effect of incorporating the high density hydrophilic graphene oxide on the water adsorption and thermal conductivity of MIL-101(Cr). Two methods were used to develop a composite of MIL-101(Cr) and GrO namely; mixing the two materials and integrating them through the synthesis process. It was found that the composites produced from the mixing route gave a lower water uptake due to the low porosity of the GrO. In the synthesis approach, the 2%GrO_synthesis composite showed a similar water uptake in the low relative pressure range and outperformed the neat material at high relative pressure. The 5%GrO_synthesis composite showed a lower water uptake due to the distortion of the crystal structure.

Regarding the thermal conductivity, all the composite samples outperformed the parent neat material as the thermal conductivity increased by up to 2.5 folds in case of the 5%GrO_physical composite and almost 20−30% increase in case of the 2%GrO composites. For the 2%GrO_synthesis composite, introducing GrO to the neat MIL-101(Cr) improved the water adsorption characteristics and significantly enhanced the heat transfer properties. This improvement in thermal conductivity can improve the heat transfer between the heating and cooling fluids and the MOF adsorbent material in the adsorbent beds thus improving the system outputs.

References

[1] Yoon M, Srirambalaji R and Kim K, Homochiral Metal–Organic Frameworks for Asymmetric Heterogeneous, Catalysis, Chem. Rev. 2012; 112:1196-1231.

[2] Suh M, Park H, Prasad T and Lim D, Hydrogen Storage in Metal–Organic Frameworks, Chem. Rev. 2012; 112:782-835.

[3] Kreno L, Leong K, Farha O, Allendorf M, van Duyne R and Hupp J, Metal–Organic Framework Materials as Chemical Sensors, Chem. Rev. 2012;112:1105-1125.

[4] Jeremias F, Frohlich D, Janiak C and Henninger S.K, Advancement of sorption-based heat transformation by a metal coating of highly-stable, hydrophilic aluminium fumarate MOF, RSC Adv., 2014; 4, 24073–24082.

[5] Rezk A, Al-Dadah R, Mahmoud S and Elsayed A, Characterisation of metal organic frameworks for adsorption cooling, International Journal of Heat and Mass Transfer 2012;55:7366–7374.

[6] Rezk A, Al-Dadah R, Mahmoud S and A. Elsayed, Experimental investigation of metal organic frameworks characteristics for water adsorption chillers, Proc IMechE Part C: J Mechanical Engineering Science 2013; 1–14.

[7] Jeremias F, Khutia A, Henninger S. K and Janiak C, MIL-100(Al, Fe) as water adsorbents for heat transformation purposes—a promising application, J. Mater. Chem., 2012;22:10148–10151.

[8] Henninger S. K, Habib H. A and Janiak C, MOFs as Adsorbents for Low Temperature Heating and Cooling Applications J. AM. CHEM. SOC. 2009; 131:2776–2777.

[9] Henninger S. K., Jeremias F., Kummer H. and Janiak C., MOFs for Use in Adsorption Heat Pump Processes, Eur. J. Inorg. Chem. 2012: 2625–2634.

[10] Ehrenmann J, Henninger S and Janiak C, Water Adsorption Characteristics of MIL-101 for Heat-Transformation Applications of MOFs, Eur. J. Inorg. Chem 2011;4:471–474.

[11] Rui Z, Li Q, Cui Q, Wang H,Chen H and Yao H, Adsorption Refrigeration Performance of Shaped MIL-101-Water Working Pair, Chin. J. Chem. Eng. 2014;22(5): 570-575.

[12] Khutia A, Rammelberg H.U, Schmidt T, Henninger S and Janiak C, Water Sorption Cycle Measurements on Functionalized MIL-101Cr for Heat Transformation Application, Chem. Mater. 2013; 25:790−798.

[13] Janiak C and Henninger S.K, Porous Coordination Polymers as Novel Sorption Materials for Heat Transformation Processes, Chimia 2013;67:419–424.

[14] Purewal J, Liu D, Sudik A, Veenstra M, Yang J, Maurer S, Muller U and Siegel D. J, Improved Hydrogen Storage and Thermal Conductivity in High-Density MOF‑5 Composites, J. Phys. Chem. C 2012; 116, 20199−20212.

[15] Musyoka N. M, Ren J, Annamalai P, Langmi H. W, North B. C, Mathe M and Bessarabov D, Synthesis of a hybrid MIL-101(Cr)/ZTC composite for hydrogen storage applications, Research on Chemical Intermediates, 2015;1-9.

[16] Kumar R, Jayaramulu K, Maji T. K and Rao C. N. R,Hybrid nanocomposites of ZIF-8 with graphene oxide exhibiting tunable morphology, significant CO_2 uptake and other novel properties, Chem. Commun., 2013;49:4947-4949.

[17] Petit C and Bandosz T. J, Exploring the coordination chemistry of MOF–graphite oxide composites and their applications as adsorbents, Dalton Trans., 2012;41:4027–4035.

[18] Petit C , Levasseur B, Mendoza B and Bandosz T. J, Reactive adsorption of acidic gases on MOF/graphite oxide composites , Microporous and Mesoporous Materials, 2012; 154:107–112.

[19] Bandosz T. J, Petit C, MOF/graphite oxide hybrid materials: exploring the new concept of adsorbents and catalysts, Adsorption, 2011;17: 5–16.

[20] Petit C and Bandosz T. J, Synthesis, Characterization, and Ammonia Adsorption Properties of Mesoporous Metal–Organic Framework (MIL(Fe))–Graphite Oxide Composites: Exploring the Limits of Materials Fabrication, Adv. Funct. Mater., 2011;21:2108–2117.

[21] Petit C and Bandosz T. J, MOF–graphite oxide nanocomposites: surface characterization and evaluation as adsorbents of ammonia, J. Mater. Chem., 2009;19:6521–6528.

[22] Xiang Z, Hu Z, Cao D, Yang W, Lu J, Han B, Wang W, Metal–Organic Frameworks with Incorporated Carbon Nanotubes: Improving Carbon Dioxide and Methane Storage Capacities by Lithium Doping, Angew. Chem., 2011;123:511 –514.

[23] Sheykhi S, Anbia M, Rashidi A. M, Shiri Garakani A. R, Mandegarzad S, Proceedings of the 4th International Conference on Nanostructures (ICNS4), 2012, Kish Island, I.R. Iran

[24] Zhou X, Huang W, Shi J, Zhao Z, Xia Q, Li Y, Wang H and Li Z, A novel MOF/graphene oxide composite GrO@MIL-101 with high adsorption capacity for acetone, J. Mater. Chem. A, 2014; 2:4722–4730.

[25] Sun X, Li Y, Xi H and Xia Q, Adsorption performance of a MIL-101(Cr)/graphite oxide composite for a series of n-alkanes, RSC Adv., 2014;4:56216–56223.

[26] Yan J, Yu Y, Ma C, Xiao J, Xia Q, Li Y and Li Z, Adsorption isotherms and kinetics of water vapour on novel adsorbents MIL-101(Cr)@GO with super-high capacity, Applied Thermal Engineering, 2015;84:118-125.

[27] Zhang X and Jiang J, Thermal Conductivity of Zeolitic Imidazolate Framework-8: A Molecular Simulation Study, J. Phys. Chem. C, 2013;117:18441−18447.

[28] Liu D, Purewal J.J, Yang J, Sudik A, Maurer S, Mueller U, Ni J and Siegel D.J, MOF-5 composites exhibiting improved thermal conductivity, International Journal of Hydrogen Energy, 2012; 37:6109-6117.

[29] Im H and Kim J, Thermal conductivity of a graphene oxide–carbon nanotube hybrid/epoxy composite, Carbon, 2012;50:5429-5440.

[30] Wang W, Wang C, Wang T, Li W, Chen L, Zou R, Zheng J and Li X, Enhancing the thermal conductivity of n-eicosane/silica phase change materials by reduced graphene oxide, Materials Chemistry and Physics, 2014;147:701-706.

[31] Hadadian M, Goharshadi E.K and Youssefi A, Electrical conductivity, thermal conductivity and rheological properties of graphene oxide-based nanofluids, J. Nanopar.t Res., 2014;16:2788.

[32] Zhou T, Liu F, Suganuma K and Nagao, Use of graphene oxide in achieving high overall thermal properties of polymer for printed electronics, RSC Adv., 2016;6:20621–20628.

[33] Wang S, Tambraparni M, Qiu J, Tipton J and Dean D, Thermal Expansion of Graphene Composites, Macromolecules, 2009;42:5251–5255.

[34] Yang J, Zhao Q, Li J and Dong J, Synthesis of metal–organic framework MIL-101 in TMAOH-$Cr(NO_3)_3$-H_2BDC-H_2O and its hydrogen-storage behaviour, Microporous and Mesoporous Materials, 2010;130:174–179.

[35] Brunauer S, Emmett P and Teller E, Adsorption of Gases in Multimolecular Layers, J. Am. Chem. Soc.,1938;60:309-319.

[36] Sun X, Xia Q, Zhao Z, Li Y and Li Z, Synthesis and adsorption performance of MIL-101(Cr)/graphite oxide composites with high capacities of n-hexane, Chemical Engineering Journal, 2014;239:226–232.

[37] Canivet J, Fateeva A, Guo Y, Coasne B and Farrusseng D, Water adsorption in MOFs: fundamentals and applications, Chem. Soc. Rev., 2014;43:5594—5617.

[38] Furukawa H, Gandara F, Zhang Y, Jiang J, Queen W. L, Hudson M. R and Yaghi O. M, Water Adsorption in Porous Metal−Organic Frameworks and Related Materials, J. Am. Chem. Soc. 2014, 136, 4369−4381.

[39] Mahanta N. K and Abramson A. R, Thermal Conductivity of Graphene and Graphene Oxide Nanoplatelets, 2012, l3th IEEE ITHERM Conference.

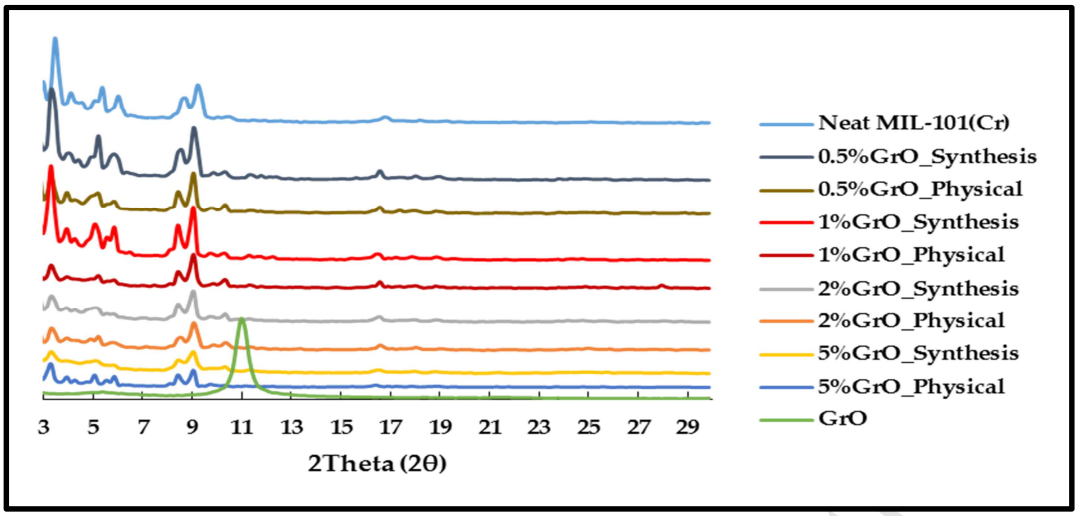

Fig.1 Powder XRD patterns of MIL-101(Cr), GrO and different composites.

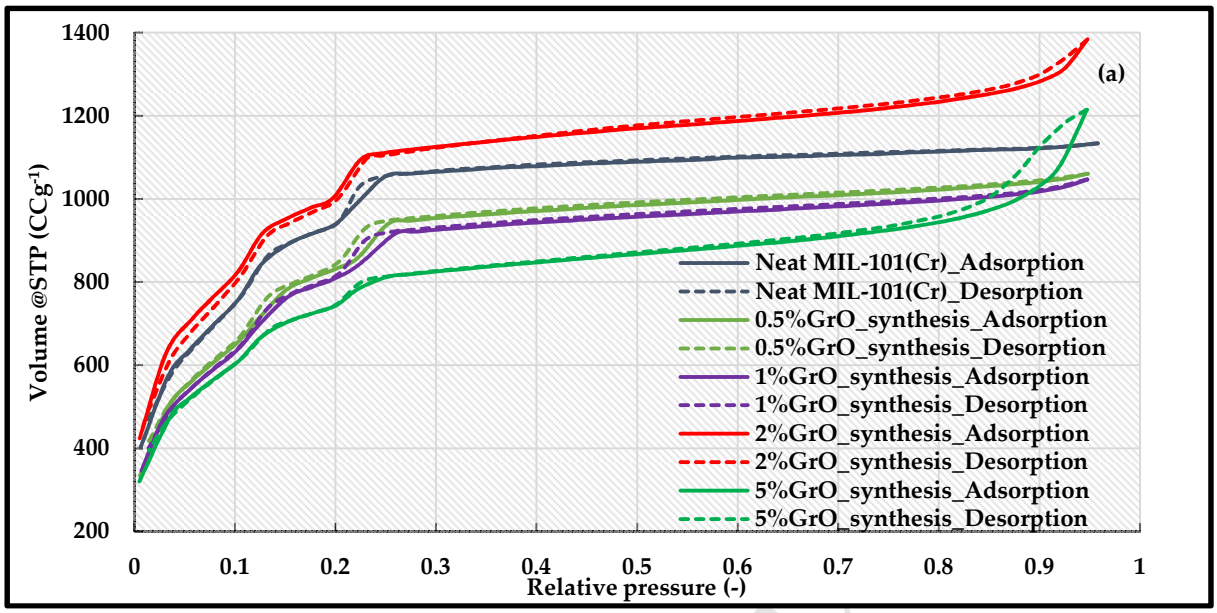

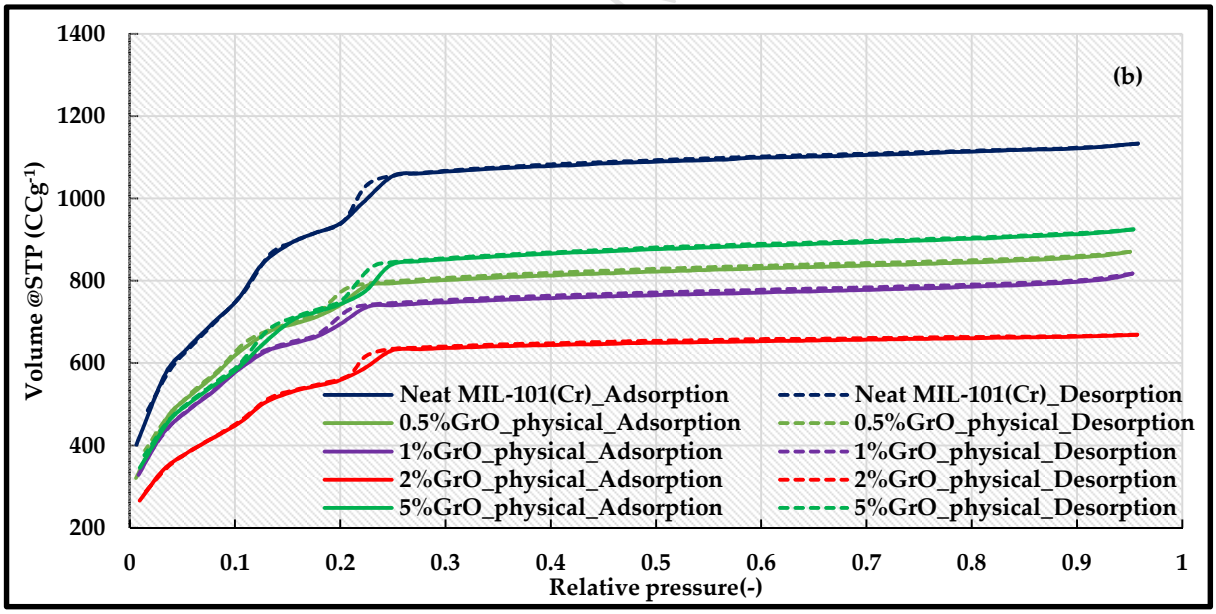

Fig.2 Nitrogen adsorption isotherms of MIL-101(Cr), a. synthesis composites and b. physical composites at 77K.

Fig.3 GrO layer, MIL-101(Cr) cage and configuration of the GrO layer on the MIL-101(Cr) at different concentrations.

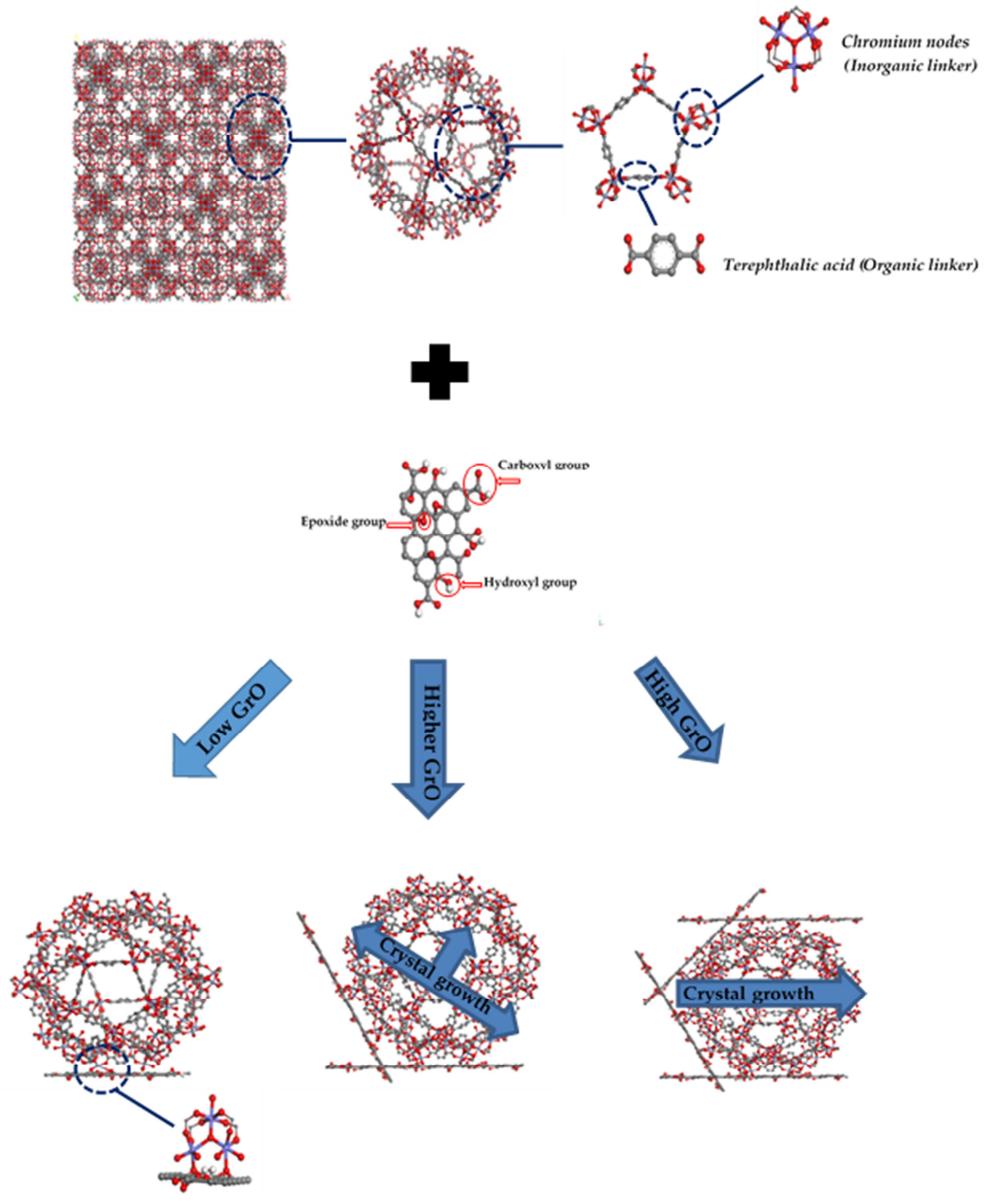

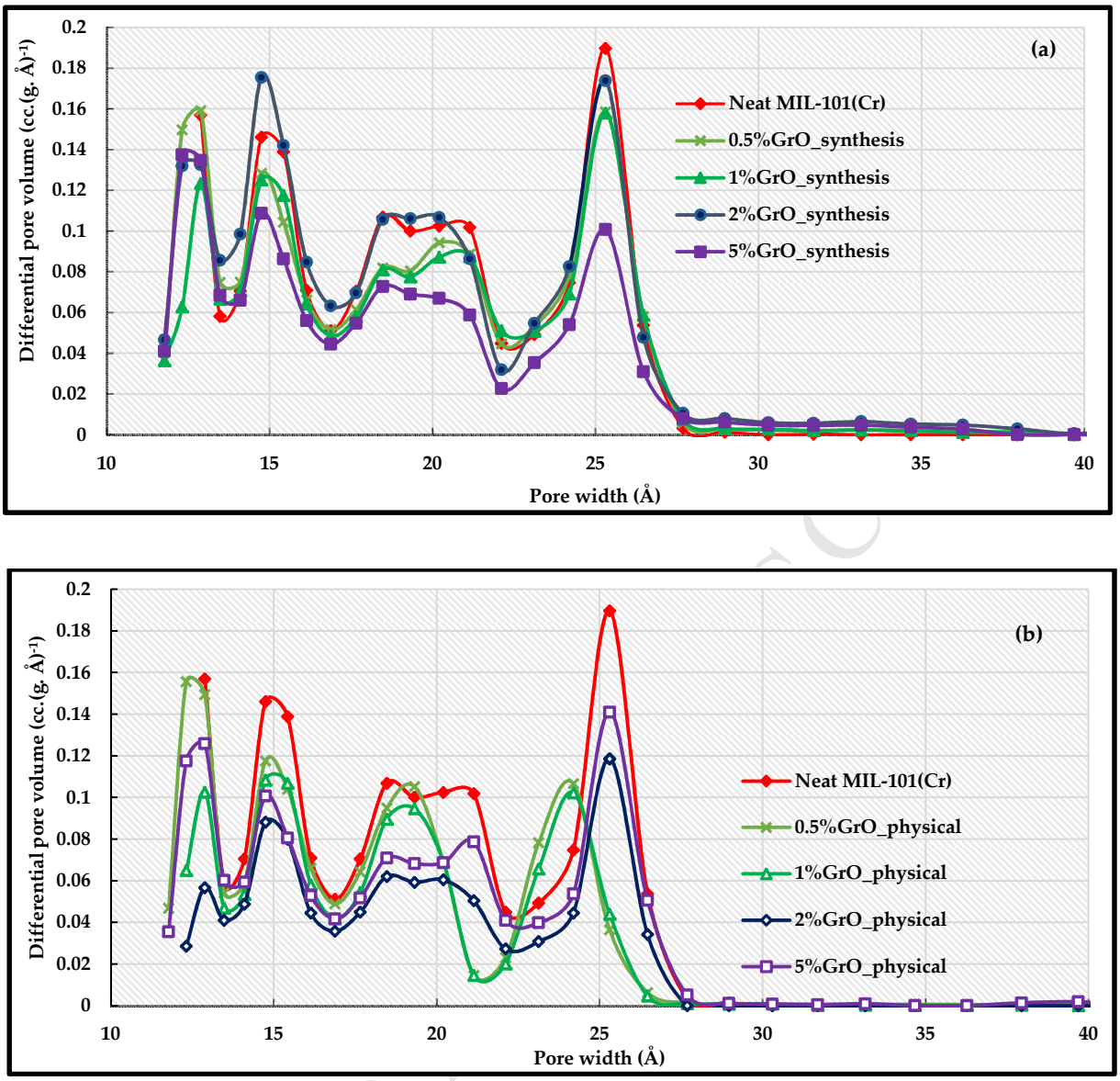

Fig.4 Pore size distribution of MIL-101(Cr), a. synthesis composites and b. physical composites.

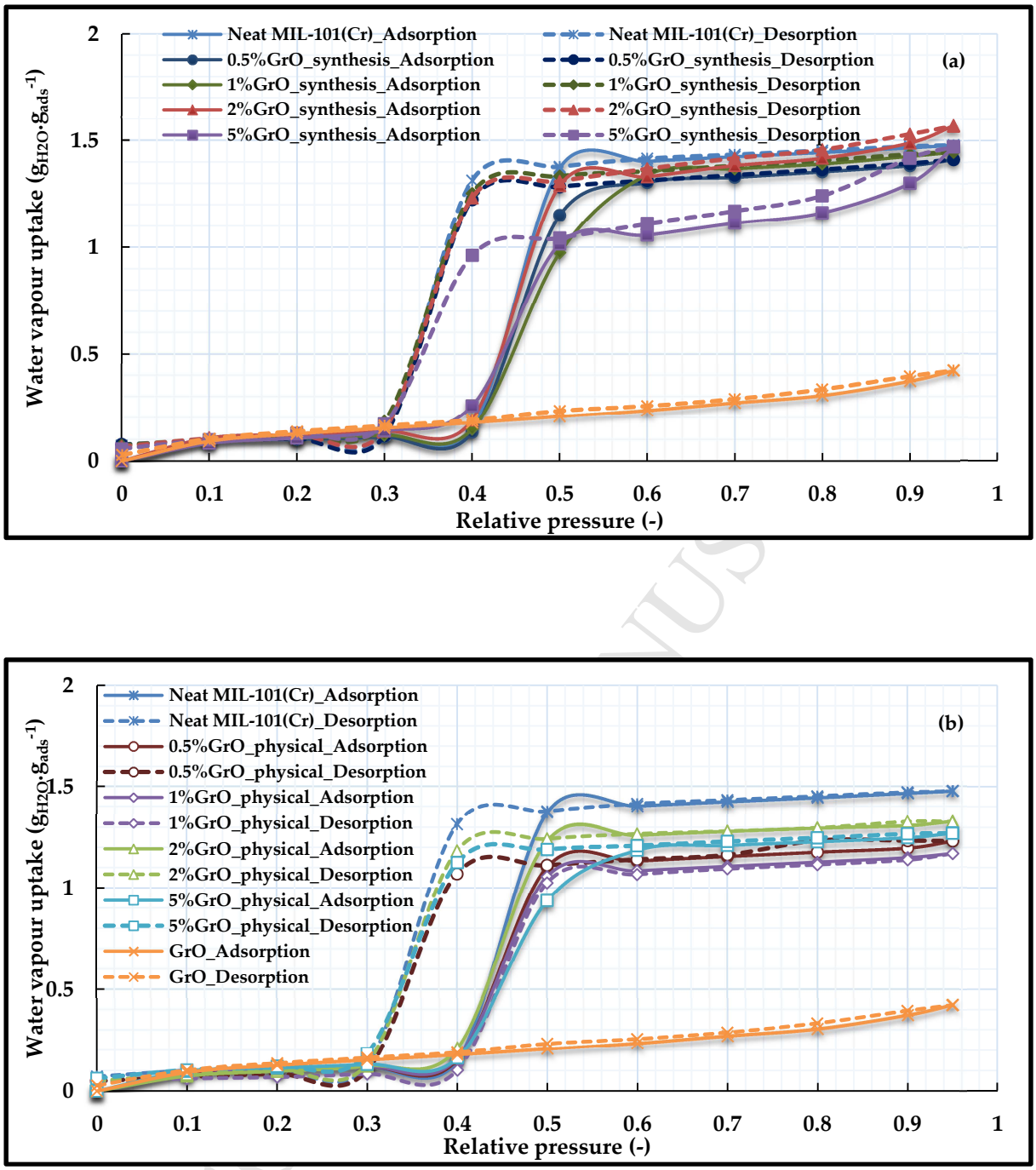

Fig.5 Water adsorption isotherms of neat MIL-101(Cr), GrO and a. synthesis composites and b. physical composites at 298 K.

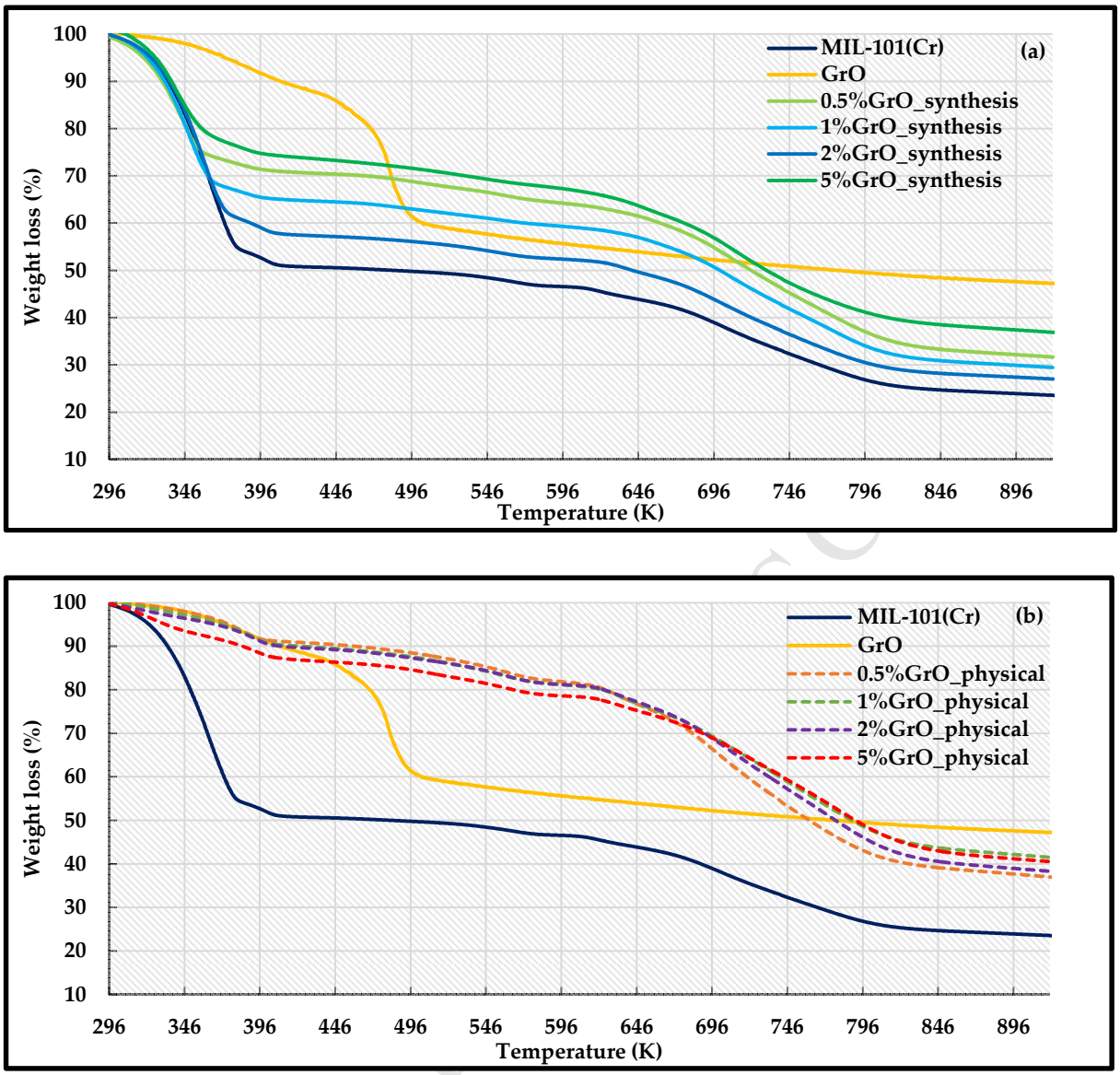

Fig. 6 Thermogravimetric analysis of MIL-101(Cr), GrO, a. synthesis composites and b. physical composites.

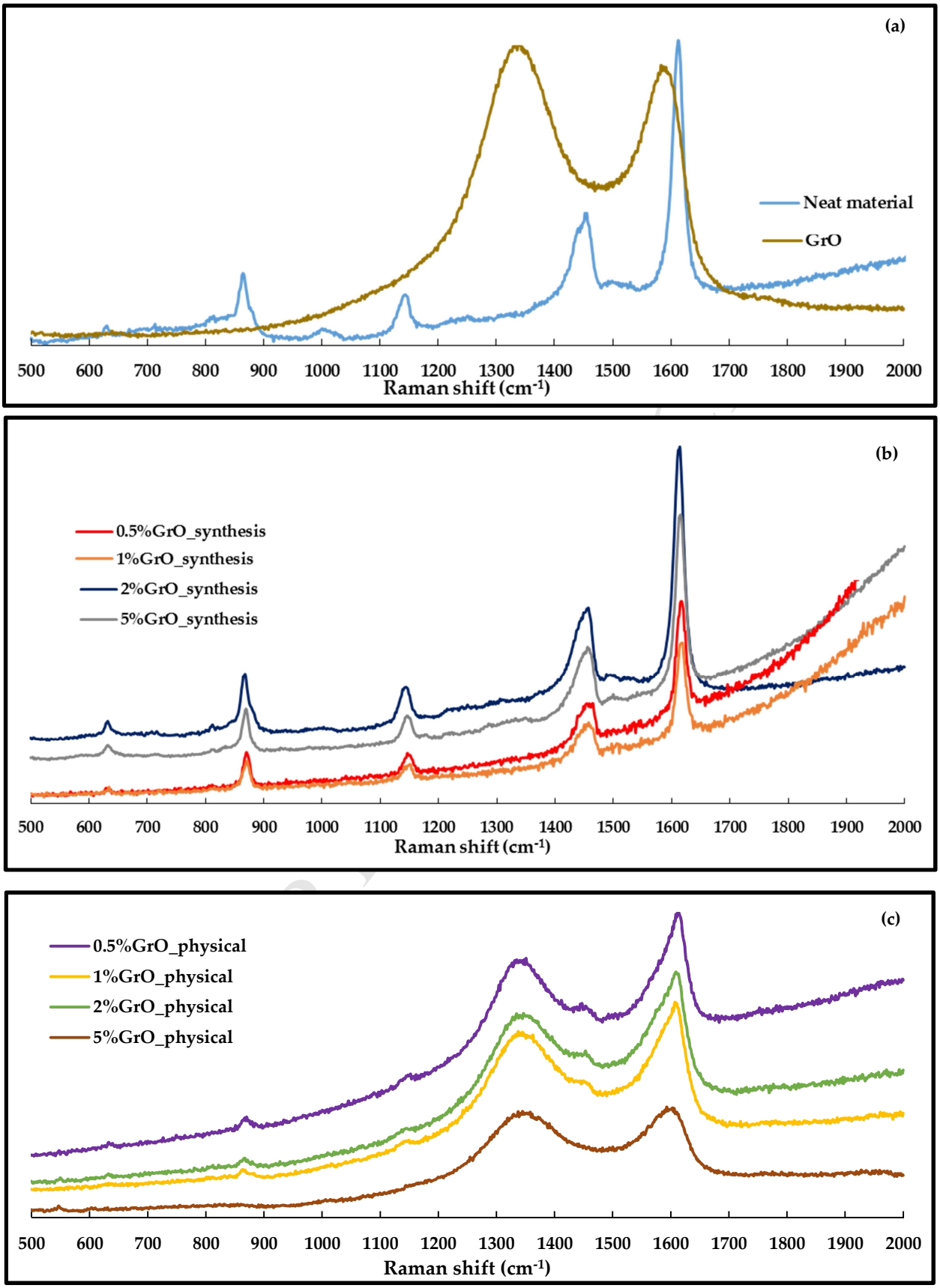

Fig.7 Raman spectra of a. MIL-101(Cr) and GrO, b. synthesis_composites and c. physical_composites.

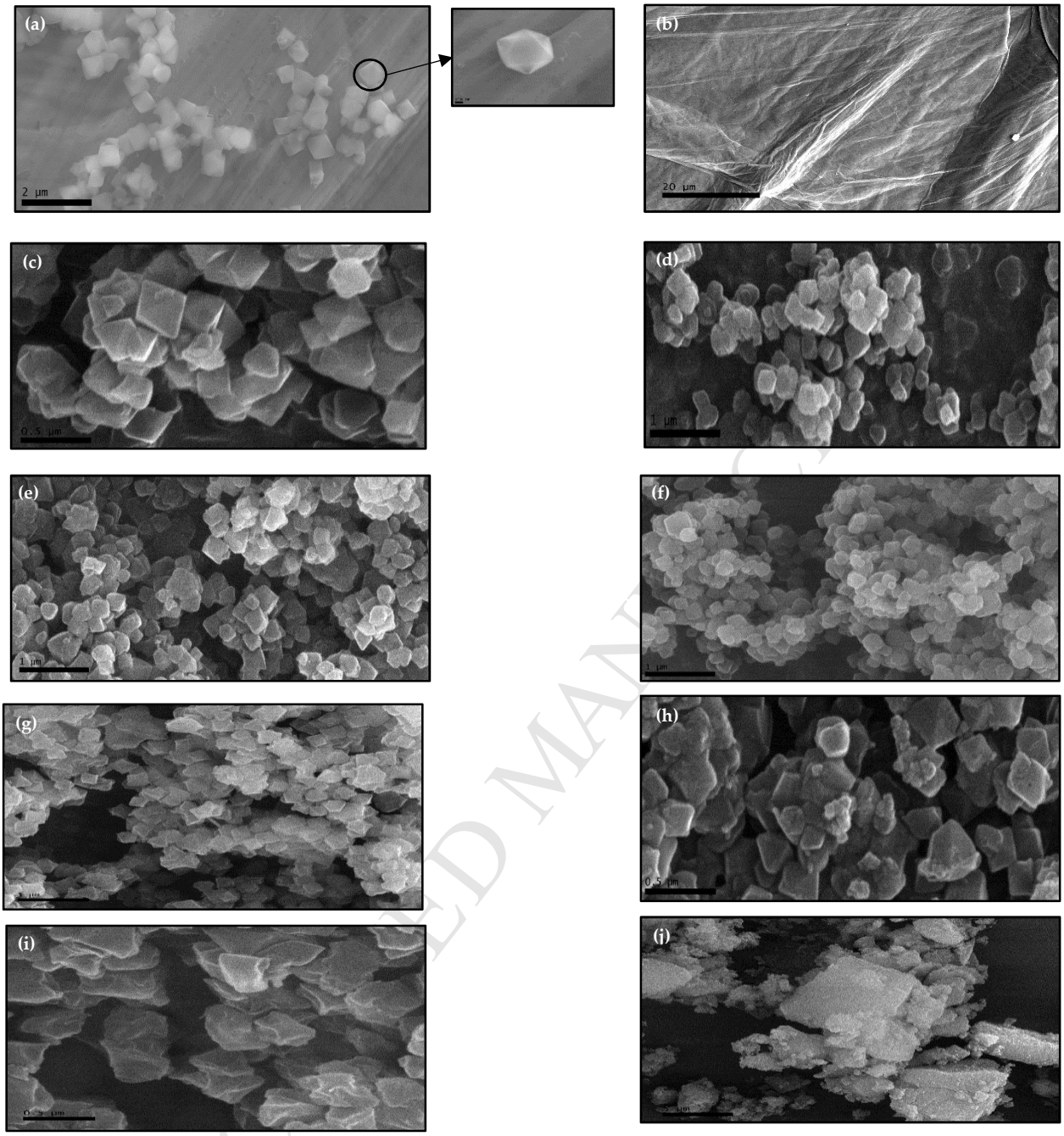

Fig. 8 SEM images of a. MIL-101(Cr), b. GrO, c. 0.5%GrO_synthesis, d. 0.5%GrO_physical, e. 1%GrO_synthesis, f. 1%GrO_physical, g. 2%GrO_synthesis, h. 2%GrO_physical, i. 5%GrO_synthesis and j. 5%GrO_physical .

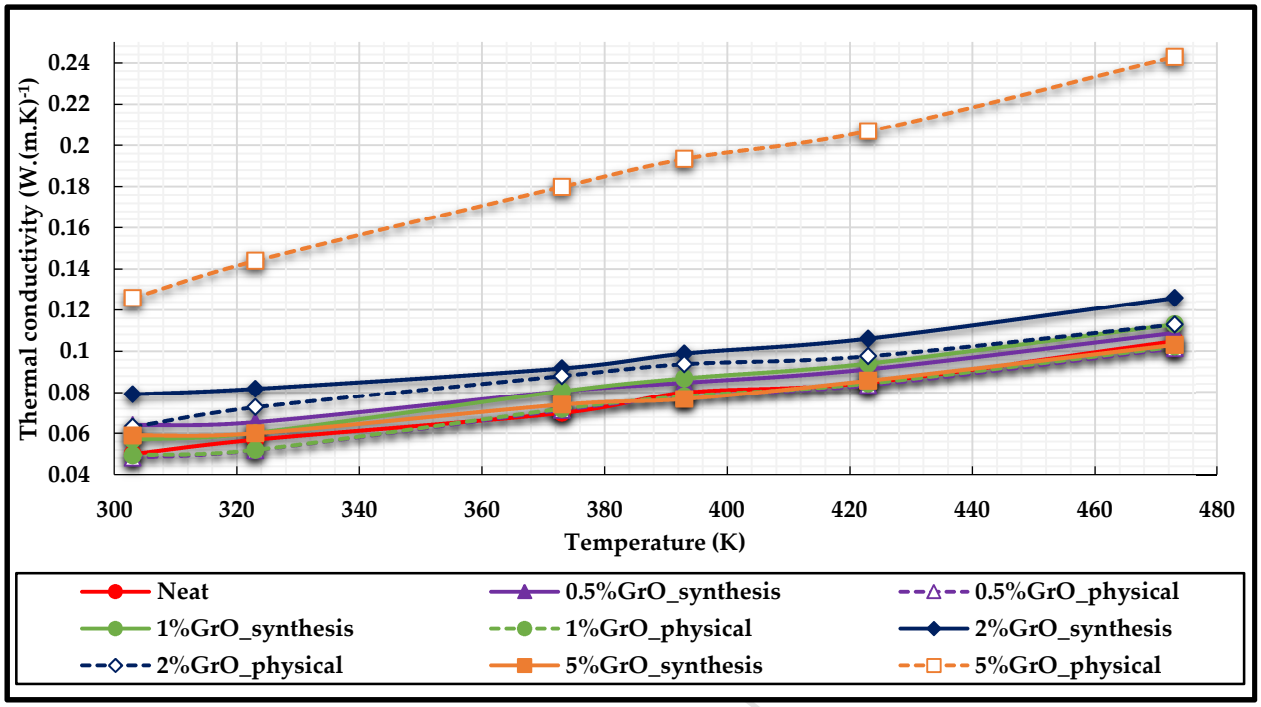

Fig.9 Thermal conductivity of MIL-101(Cr) and MIL/GrO composites.

Highlights:

- Composites MIL-101(Cr)/Graphene oxide were synthesized with different GrO content.
- The 2%GrO_synthesis composite showed enhanced water adsorption characteristics.
- MIL-101/GrO showed higher thermal conductivity than parent material.
- MIL-101/GO is a promising candidate for adsorption heat pump applications.